

X-ray Rietveld and ^{57}Fe Mössbauer studies of epidote and piemontite on the join $\text{Ca}_2\text{Al}_2\text{Fe}^{3+}\text{Si}_3\text{O}_{12}(\text{OH})\text{--Ca}_2\text{Al}_2\text{Mn}^{3+}\text{Si}_3\text{O}_{12}(\text{OH})$ formed by hydrothermal synthesis

MARIKO NAGASHIMA^{1,2,*} AND MASAHIDE AKASAKA¹

¹Department of Geoscience, Faculty of Science and Engineering, Shimane University, Matsue 690-8504, Japan

²Mineralogical Crystallography, Institute of Geological Sciences, University of Bern, Freiestrasse 3, CH-3012 Bern, Switzerland

ABSTRACT

Fe^{3+} and Mn^{3+} distributions on octahedral M1, M2, and M3 sites in synthetic epidote/piemontite from $\text{Ca}_2\text{Al}_2\text{Fe}_q^{3+}\text{Mn}_{1-q}^{3+}\text{Si}_3\text{O}_{12.5}$ starting material and their effects on the crystal structure were investigated using X-ray Rietveld and ^{57}Fe Mössbauer methods. Epidote and piemontite were crystallized as almost single phases from $q = 1.0, 0.75, 0.5,$ and 0.25 starting materials at P_{fluid} of 200–400 MPa and a temperature of 500 °C, using standard cold-seal pressure vessels. The $\text{Mn}_2\text{O}_3\text{--MnO}_2$ buffer was used to produce f_{O_2} adequate to maintain Fe^{3+} and Mn^{3+} . The Rietveld refinements converged to goodness-of-fit ranges from 1.21 to 1.60.

At this temperature, site preferences of $\Sigma(\text{Fe}^{3+}+\text{Mn}^{3+})$ for octahedral sites are $\text{M3} > \text{M1} (>> \text{M2})$. K_D values of $\Sigma(\text{Fe}^{3+}+\text{Mn}^{3+})$, where $K_D = [(\text{Fe}^{3+}+\text{Mn}^{3+})/\text{Al}]^{\text{M1}}/[(\text{Fe}^{3+}+\text{Mn}^{3+})/\text{Al}]^{\text{M3}}$, (0.05–0.13) are similar to those of individual Mn^{3+} and Fe^{3+} vs. Al^{3+} , respectively. However, the K_D values of Fe^{3+} and Mn^{3+} for M1 and M3, where $K_D = (\text{Fe}^{3+}/\text{Mn}^{3+})^{\text{M1}}/(\text{Fe}^{3+}/\text{Mn}^{3+})^{\text{M3}}$, vary with $\text{Fe}_{\text{Total}}^{3+}:\text{Mn}_{\text{Total}}^{3+}$ ratios. In epidote with Fe^{3+} content larger than 0.4 atoms per formula unit (apfu) and $\text{Mn}^{3+} < 0.6$ apfu, Fe^{3+} has a stronger preference for M1 than Mn^{3+} . In piemontite with 0.12 Fe^{3+} and 0.73–0.78 Mn^{3+} apfu, the preference of Mn^{3+} for M1 is greater than that of Fe^{3+} . The site occupancies of individual Mn^{3+} and Fe^{3+} are governed by the individual K_D values and the Mn^{3+} and Fe^{3+} concentrations in corresponding epidote and piemontite. Variations of the unit-cell parameters indicate the combined result of linear variation due to $\text{Al} \leftrightarrow \text{Fe}^{3+}$ substitution and nonlinear variation due to $\text{Al} \leftrightarrow \text{Mn}^{3+}$ substitution.

Keywords: Epidote, piemontite, synthesis, Rietveld refinement, Mössbauer spectroscopy

INTRODUCTION

Epidote-group minerals are important rock-forming phases occurring in a variety of geological conditions. The general formula of epidote-group minerals is $\text{A1A2M1M2M3Z}_3\text{O}_{12}(\text{OH})$. The main components of most epidote and piemontite are $\text{Ca}_2\text{Al}_3\text{Si}_3\text{O}_{12}(\text{OH})$, $\text{Ca}_2\text{Al}_2\text{Fe}^{3+}\text{Si}_3\text{O}_{12}(\text{OH})$, and $\text{Ca}_2\text{Al}_2\text{Mn}^{3+}\text{Si}_3\text{O}_{12}(\text{OH})$. Ca^{2+} occupies 9-coordinated A1 and 10-coordinated A2 sites; Al, Mn^{3+} , and Fe^{3+} are distributed over octahedral M1, M2, and M3 sites, and Si cations occur at the tetrahedral Z site. The octahedral sites form two types of chains of edge-sharing octahedra: a single chain of M2 octahedra and a multiple chain with central M1 and peripheral M3 octahedra (Ito et al. 1954; Dollase 1968, 1969, 1971). The M3 octahedron is larger and more distorted than M1 and M2. The volumes of the three crystallographically independent octahedra vary as $\text{M3} > \text{M1} > \text{M2}$, where M2 is the smallest and least distorted octahedron.

The distribution of Mn^{3+} and Fe^{3+} among the three types of octahedral sites and the structural changes caused by Mn^{3+} and/or Fe^{3+} substitution for Al in epidote-group minerals have been investigated by single-crystal structure refinements (Dollase 1969, 1971; Kvik et al. 1988; Ferraris et al. 1989; Bonazzi et al. 1990, 1992; Bonazzi and Menchetti 1994, 1995; Giuli et al. 1999; Langer et al. 2002; and others) and X-ray Rietveld refine-

ment (Nagashima and Akasaka 2004). The crystal chemistry of natural epidote-group minerals has also been investigated using a variety of spectroscopic methods (Burns and Strens 1967; Dollase 1973; Paesano et al. 1983; Fehr and Heuss-Assbichler 1997; Taran and Langer 2000; Langer et al. 2002). However, it is a challenge to investigate the specific influence of unique Fe^{3+} and Mn^{3+} substitution for Al on structural changes because natural epidote-group minerals commonly contain not only Fe^{3+} but also Mn^{3+} . Although Fe^{3+} and Mn^{3+} have similar ionic radii, their electronic configurations and induced distortions are different. Moreover, Sr and REE often occur at the A sites. High Sr and/or Ba contents at A2 are known to promote the incorporation of transition elements rather than Al at the octahedral sites (Armbruster et al. 2002; Nagashima and Akasaka 2004; Fukushima et al. 2005). Therefore, the influence of Fe^{3+} or Mn^{3+} substitution for Al was investigated in synthetic pure Al- Fe^{3+} and Al- Mn^{3+} binary series, respectively, by Anastasiou and Langer (1977), Giuli et al. (1999), Langer et al. (2002), and Nagashima and Akasaka (2004). However, the intracrystalline partitioning of Fe^{3+} and Mn^{3+} in pure Al- Fe^{3+} - Mn^{3+} ternary series has not yet been examined.

In this study, we investigate the distribution of Fe^{3+} and Mn^{3+} among octahedral sites and the variations of structural changes caused by Fe^{3+} and Mn^{3+} substitution for Al. Unit-cell parameters and interatomic distances and angles are measured on a synthetic Al- Fe^{3+} binary series and a Al- Fe^{3+} - Mn^{3+} ternary series of epidote-group minerals from $\text{Ca}_2\text{Al}_2\text{Fe}_q^{3+}\text{Mn}_{1-q}^{3+}\text{Si}_3\text{O}_{12.5}+\text{H}_2\text{O}$ for starting materials with $q = 1.0, 0.75, 0.5,$ and 0.25 .

* Present address: Department of Earth Science, Graduate School of Science and Engineering, Yamaguchi University, 753-8512, Japan. E-mail: nagashim@yamaguchi-u.ac.jp

EXPERIMENTAL METHODS

Details of the syntheses have been reported by Nagashima (2006). The starting materials for this study consisted of mixtures of synthetic CaFe³⁺[AlSiO₆]-pyroxene (esseneite) and oxides. Appropriate amounts of esseneite, CaCO₃, Al₂O₃, MnO₂, and SiO₂-reagents were mixed to produce compositions of Ca₂Al₂Fe³⁺Mn³⁺_{1-q}Si₃O_{12.5}, where $q = 1.0, 0.75, 0.5, \text{ and } 0.25$. The starting materials were sealed in Ag₉₀Pd₁₀ capsules containing excess distilled water. The Mn₂O₃-MnO₂ buffer was used to produce f_{O_2} adequate to maintain Fe³⁺ and Mn³⁺. Hydrothermal syntheses were carried out at P_{fluid} of 200–400 MPa and a temperature of 500 °C using standard cold-seal hydrothermal pressure vessels.

The chemical compositions of synthetic phases were analyzed using a JEOL JXA-8800M electron microprobe analyzer (EMPA) operating at 15 kV, with a beam current of 20 nA, and beam diameter of 1 μm. Standards used were wollastonite and epidote for Ca and Si, synthetic MnO for Mn, synthetic hematite for Fe, and synthetic Al₂O₃ and epidote for Al. The ZAF method was used for data correction.

To avoid preferred orientation effects, grinding samples to a very small particle size with less than 10 μm is one of the most critical requirements for any structure study based on powder X-ray diffraction data (Bish and Reynolds 1989; Post and Bish 1989). To achieve this, the samples were manually finely ground under alcohol in an agate mortar until the resultant particle sizes were <5 μm, which was confirmed using an optical microscope. Powdered samples were mounted on glass sample holders with a 20 × 15 × 0.5 mm notch. Mounts for intensity profile collection were made by loading the powder from the front of the holder. Following the method of Raudsepp et al. (1990), a straight edge was used to level the sample surface to that of the holder. The surface was then finely serrated several times with a razor blade. This technique tends to randomize the orientation of anisotropic crystals that are aligned during filling, while maintaining a generally flat surface.

Step-scan powder diffraction data were collected using a RIGAKU RINT automated X-ray powder diffractometer with a Bragg-Brentano goniometer equipped with incident- and diffracted-beam soller slits, 1° divergence and anti-scatter slits, a 0.15 mm receiving slit, and a curved graphite diffracted-beam monochromator. The normal-focus Cu X-ray tube for CuKα line was operated at 40 kV and 25 mA. Profiles were taken between 10 and 150 °2θ with a step interval of 0.02 °2θ, using step counting times that accumulated around 5000 counts for the strongest peaks.

Crystal structures of the synthetic phases were refined using the RIETAN-2000 program of Izumi and Ikeda (2000). Single-crystal X-ray results for epidote and piemontite (Dollase 1969, 1971), hematite (Blacke et al. 1966), bixbyite (Geller 1971), and esseneite (Cosca and Peacor 1987) were used as the initial parameters for the Rietveld refinement. The cell parameters of epidote and piemontite were determined with a program in the RIGAKU RINT system. They were used as initial values. Based on the result of the chemical analysis, Ca occupancy at A1 and A2 and Si occupancy at Z were fixed at 1, respectively. Although synthetic epidote and piemontite containing very small amounts of Fe³⁺ or Mn³⁺ at M2 have been reported (Giuli et al. 1999; Nagashima and Akasaka 2004), the occupancy at M2 was fixed to 1.0 Al atom on the basis of single-crystal studies for natural epidote and piemontite (e.g., Dollase 1969, 1971). Because Fe and Mn cannot be distinguished on the basis of their X-ray atomic scattering factors, total Fe+Mn was refined applying the scattering factor of Mn, and is represented as M³⁺. In the refinement, the scattering factors of neutral atoms were employed for all elements. Occupancy factors for Al and M³⁺ on octahedral sites were refined using the following constraints: $M_{M2}^{3+} = M_{\text{total}}^{3+} - M_{M1}^{3+}$, $Al_{M1} = 1.0 - M_{M1}^{3+}$, and $Al_{M3} = 1.0 - M_{M3}^{3+}$, where M_{total}^{3+} is the $\Sigma(\text{Fe}^{3+} + \text{Mn}^{3+})$ value determined by EMPA analysis. All isotropic displacement parameters were fixed to those obtained in single-crystal studies (Dollase 1969, 1971). Peaks were defined using a "Modified split pseudo-Voigt" function, which comprised the split pseudo-Voigt function of Toraya (1990) combined with profile relaxation or the Pearson VII function in RIETAN-2000. An asymmetry parameter was built into this profile function. Details of these profile functions are given by Izumi and Ikeda (2000). Nonlinear least-squares calculation using the Marquardt method was followed by the conjugate-direction method to check convergence at local minima (Izumi 1993). Preferred orientation was corrected using the March-Dollase function (Dollase 1986).

The ⁵⁷Fe Mössbauer transmission spectra were recorded at room temperature using a constant acceleration spectrometer, a multichannel analyzer with 1024 channels and a ⁵⁷Co/Pd source (=370 MBq). The absorbers were about 150 mg of powder samples, which were settled on adhesive tape with 1 cm in diameter and <0.5 mm in thickness. Velocity calibration was done using a metallic Fe foil, and the Mössbauer parameters such as isomer shift (IS) and quadrupole splitting (QS) are given relative to this standard. The spectra were fitted to Lorentzian curves using the least-squares method with line widths and intensities constrained to be

equal at each site. The QBMOSS program written by Akasaka and Shinno (1992) was used for computer numerical analysis. The quality of the fit was judged using the χ^2 value and standard deviations of Mössbauer parameters. Errors of the Mössbauer hyperfine parameters were calculated from the standard deviations (1σ) of peak positions, peak widths, and intensities.

RESULTS

Syntheses

The experimental conditions and results of the syntheses are listed in Table 1. Details of the syntheses were reported by Nagashima (2006). The product from $q = 1.0$ starting material at 400 MPa and 500 °C (run no. 41) was yellowish green in color, and was composed mainly of epidote with associated trace amounts of hematite. The synthetic epidote crystals were yellowish green to brownish green and prismatic up to 50 μm × 10 μm. In contrast, the products from the Mn³⁺-bearing starting materials were brownish purple to purple, and pure Al-Fe³⁺-Mn³⁺ piemontite was produced more readily. The product from $q = 0.75$ at 360 MPa and 500 °C (run no. 27) was mainly composed of epidote. The product from $q = 0.5$ at 200 MPa and 500 °C (run no. 22) was only composed of Al-Fe³⁺-Mn³⁺ piemontite, that at 360 MPa and 500 °C (run no. 21) consisted mainly of Al-Fe³⁺-Mn³⁺ piemontite and trace hematite. The products from $q = 0.25$ at 200 MPa and 370 MPa and 500 °C (run nos. 38 and 30) also consisted mainly of Al-Fe³⁺-Mn³⁺ piemontite. They were associated with trace amounts of bixbyite (run no. 38) and trace hematite (run no. 30). Esseneite, which is relict of the starting material, was found in the products of run nos. 41, 27, 21, and 38.

Chemical compositions of synthetic epidote/piemontite

The chemical compositions of epidote from run no. 41 and piemontite from run nos. 27, 22, 38, and 30 are listed in Table 2, where total Fe and Mn are shown as Fe₂O₃ and Mn₂O₃, respectively. The chemical compositions of synthetic phases in run no. 21 product were unable to be analyzed because of very fine grain sizes. The oxidation state of Fe was confirmed by ⁵⁷Fe Mössbauer spectroscopy. The Fe oxidation state of the products from run nos. 27, 22, 21, 38, and 30 is only Fe³⁺. On the other hand, trace amounts of Fe²⁺ (4% of total Fe) was detected in the product from run no. 41, but Fe²⁺ is considered to be negligible.

Epidote from run no. 41, which crystallized along with a trace amount of hematite, has nearly the same cation ratio as the starting material: Ca:Fe³⁺:Al:Si = 1.99:0.91:2.10:2.99. The chemical compositions of Al-Fe³⁺-Mn³⁺ piemontite from run nos. 27, 22, 38, and 30 were generally close to those of starting materials, except that Fe³⁺ contents tended to be slightly lower:

TABLE 1. Experimental results

Run no.*	q†	P (MPa)	T (°C)	Duration (day)	Mineral assemblage‡
41	1.0	400	500	43	Ep(+Hm)§
27	0.75	360	500	20	Ep(+Hm)§
22	0.5	200	500	34	Pm
21	0.5	360	500	17	Pm(+Hm)§
38	0.25	200	500	36	Pm(+Bx)§
30	0.25	370	500	22	Pm(+Hm)

Note: MnO₂-Mn₂O₃ buffer was used for syntheses.

* Starting materials consisting of synthetic esseneite (CaFeAlSiO₆) + oxide mixtures were used for experiments.

† $q = \text{Fe}^{3+}$ in Ca₂Al₂Fe³⁺Mn³⁺_{1-q}Si₃O_{12.5}-oxide mixture.

‡ Bx = bixbyite, Ep = epidote, Hm = hematite, Pm = piemontite.

§ Small amount of esseneite from the starting material remained.

TABLE 2. Average chemical compositions of epidote and piemontite

<i>q</i> -value*	1.0		0.75		0.5		0.25			
<i>P</i> (MPa)	400		360		200		200		370	
<i>T</i> (°C)	500		500		500		500		500	
Run no.	41		27		22		38		30	
	<i>n</i> = 28 (18 grains)		<i>n</i> = 6 (5 grains)		<i>n</i> = 10 (10 grains)		<i>n</i> = 16 (12 grains)		<i>n</i> = 6 (6 grains)	
	avg.	s.d.	avg.	s.d.	avg.	s.d.	avg.	s.d.	avg.	s.d.
SiO ₂	37.41	0.44	36.86	0.52	36.75	0.37	37.40	0.72	36.91	0.59
Al ₂ O ₃	22.26	1.67	23.28	0.44	22.18	1.04	22.45	1.16	22.15	0.57
Fe ₂ O ₃ †	15.15	2.33	9.51	1.36	6.40	1.34	2.05	0.85	2.03	0.61
Mn ₂ O ₃ †	–	–	3.37	0.98	8.57	1.86	12.86	1.63	11.68	1.28
CaO	23.16	0.45	23.69	0.46	22.71	0.36	23.28	0.53	23.08	0.62
Total	97.98	–	96.71	–	96.61	–	98.04	–	95.85	–
Cations per 12.5 O atoms										
Si	2.99	0.02	2.98	0.04	2.98	0.02	2.99	0.04	3.01	0.03
Al	2.10	0.14	2.22	0.03	2.12	0.09	2.11	0.09	2.13	0.04
Fe	0.91	0.15	0.58	0.08	0.39	0.08	0.12	0.05	0.12	0.04
Mn	–	–	0.21	0.06	0.53	0.12	0.78	0.11	0.73	0.08
Ca	1.99	0.04	2.05	0.03	1.97	0.03	1.99	0.04	2.02	0.06
Total	7.99	–	8.04	–	7.99	–	7.99	–	8.01	–

* Abbreviations as in Table 1.

† Total Fe and Mn as Fe₂O₃ and Mn₂O₃, respectively.

Al:Fe³⁺:Mn³⁺ = 2.22:0.58:0.21 for run no. 27, Al:Fe³⁺:Mn³⁺ = 2.12:0.39:0.53 for run no. 22, Al:Fe³⁺:Mn³⁺ = 2.11:0.12:0.78 for run no. 38, and Al:Fe³⁺:Mn³⁺ = 2.13:0.12:0.73 for run no. 30. Liou (1973) considered that the cause of iron loss was reducing conditions in the capsules with subsequent Fe absorption. In fact, absorption of iron by the Ag₉₀Pd₁₀ inner capsule was confirmed by EMPA. However, since the Mn₂O₃-MnO₂ buffer used in this study maintained high oxygen fugacity, the main cause of decreased Fe³⁺ in Mn³⁺-Fe³⁺-Al piemontite relative to the starting materials can be attributed to crystallization of some hematite confirmed using an optical microscope, even in the case that hematite was not necessarily detected. Our synthetic epidote and piemontite contain 1.97–2.05 Ca and 2.98–3.01 Si apfu, indicating that the A1 and A2 sites are filled with Ca²⁺ and the tetrahedral Z sites with Si⁴⁺. Thus, A1 and A2 are described as Ca1 and Ca2, and the Z as Si in the tables.

Rietveld refinement

Six run products were used for the X-ray Rietveld refinements (Table 1). Details of data collection for the Rietveld analyses, the refined mass fractions and unit-cell parameters of each phase, *R*-factors, goodness-of-fit ($S = R_{wp}/R_e$), and the Durbin-Watson *d* statistic are listed in Table 3. Because the products of run nos. 22 and 41 contained silver metal, which was dissolved from the inner capsule and precipitated in the run products, Ag-metal was added to the refinement to improve the fit. Although the refinement details for Ag-metal are not shown in Table 3, the structural parameters of silver-metal (space group *Fm* $\bar{3}$ *m*) were fixed to the initial values, and the unit-cell parameters and mass fractions were then refined, with the *a*-dimension, 4.083–4.084 Å; the mass fraction, <0.006. In the Rietveld refinements, hematite, bixbyite, and esseneite were also included as additional phases to refine the mass fractions of each phase. The Fe content was influenced by the amount of crystallized hematite and decomposed esseneite (Nagashima 2006). These facts are consistent with the results of chemical analyses of epidote and piemontite. Figure 1 shows a result of the Rietveld refinement of the product from *q* = 0.25 at 370 MPa and 500 °C (run no. 30). Despite the products of run nos. 21, 27, and 30 consist of piemontite and trace hematite (Table 1), the structural refinement was carried out as single

phase because the peaks of hematite were too small to fit. The atomic positions refined in this study are shown in Table 4¹. The crystal structure of piemontite from *q* = 0.5 starting material (run no. 22) is shown in Figure 2. The interatomic distances and selected bond angles calculated from refined atomic positions are listed in Tables 5¹ and 6¹, respectively. Errors in all tables are shown by the estimated standard deviation of 1σ (e.s.d. values). The site occupancies of M³⁺ (=Fe+Mn) are listed in Table 7. The site preference of M³⁺ is M3>M1 as well as the other trivalent transition elements such as Fe³⁺, Mn³⁺, and Cr³⁺ (i.e., Anastasiou and Langer 1977; Giuli et al. 1999; Nagashima and Akasaka 2004; Nagashima et al. 2009).

⁵⁷Fe Mössbauer spectroscopy

The ⁵⁷Fe Mössbauer spectra and hyperfine parameters of synthetic Ca₂Al₂(Fe³⁺,Mn³⁺)Si₃O₁₂(OH)-epidote/piemontite are shown in Figure 3 and Table 8, respectively. The spectrum of run no. 41 product (*q* = 1.0) composed of epidote associated with small amounts of hematite and esseneite consists of six doublets (Fig. 3a). The doublets AA' (IS = 0.36 and QS = 2.07 mm/s) and BB' (IS = 0.34 and QS = 1.55 mm/s) are assigned to Fe³⁺ at the M3 and M1 sites, respectively, because it has been known that doublets with IS = 0.24–0.44 and QS = 1.89–2.32 mm/s and IS = 0.22–0.36 and QS = 1.46–1.67 mm/s are assigned to Fe³⁺ at the M3 and M1 sites as reviewed by Liebscher (2004). The doublets CC' (IS = 0.32 and QS = 0.95 mm/s) and DD' (IS = 0.39 and QS = 0.53 mm/s) are attributed to Fe³⁺ at the octahedral M1 site in residual esseneite. The CC' value is consistent to that of synthetic esseneite (IS = 0.32–0.35 and QS = 0.9–1.0 mm/s) after Akasaka (1983, 1990). Although the doublet DD' is somewhat different from the result for synthetic esseneite, smaller QS values of Fe³⁺ at the M1 site, such as 0.72–0.80 mm/s have been also reported by Frenzel et al. (1985) and Matsui et al. (1972). Thus, the smaller QS value of Fe³⁺ of the doublet DD' may be

¹ Deposit item AM-10-039, Tables 4, 5, and 6. Deposit items are available two ways: For a paper copy contact the Business Office of the Mineralogical Society of America (see inside front cover of recent issue) for price information. For an electronic copy visit the MSA web site at <http://www.minsocam.org>, go to the *American Mineralogist* Contents, find the table of contents for the specific volume/issue wanted, and then click on the deposit link there.

TABLE 3. Data collection* and details of structure refinement

$q\bar{1}$	1.0	0.75	0.5		0.25	
Synthesis P (MPa)	400	360	200	360	200	370
T (°C)	500	500	500	500	500	500
Run no.	41	27	22	21	38	30
Fe ³⁺ ‡	0.91	0.58	0.39	0.39	0.12	0.12
Mn ³⁺ ‡	–	0.21	0.53	0.53	0.78	0.73
Total of Fe ³⁺ +Mn ³⁺	0.91	0.79	0.92	0.92	0.90	0.85
Max. intensity (counts)	4239	5724	5180	5499	6114	5964
Epidote/piemontite						
Space group	$P2_1/m$					
a (Å)	8.8902(5)	8.8980(3)	8.8817(5)	8.8904(4)	8.8831(4)	8.8727(3)
b (Å)	5.6366(2)	5.6549(2)	5.6543(3)	5.6606(2)	5.6687(3)	5.6686(2)
c (Å)	10.1600(5)	10.1752(4)	10.1630(6)	10.1760(4)	10.1715(5)	10.1682(4)
β (°)	115.432(4)	115.428(3)	115.435(4)	115.455(3)	115.450(4)	115.480(3)
V (Å ³)	459.79(4)	462.39(3)	460.91(4)	462.39(3)	462.49(4)	461.67(3)
Z	2	2	2	2	2	2
R_B (%)§	2.31	1.84	2.45	1.92	1.38	1.86
R_F (%)§	1.09	0.85	1.02	0.91	0.71	0.97
R_p (%)§	5.08	6.58	7.89	7.02	5.70	6.01
R_{wp} (%)§	6.59	8.98	10.15	9.25	7.51	7.92
R_e (%)§	5.33	6.67	6.33	6.59	5.58	6.57
S §	1.237	1.346	1.604	1.404	1.347	1.205
D-W d	1.313	1.153	0.827	1.062	1.126	1.415
Mass fraction#						
Ep, Pm	0.939	0.966	1.000	0.970	0.951	1.000
Hm	0.022					
Bx					0.020	
Es	0.039	0.034		0.030	0.028	

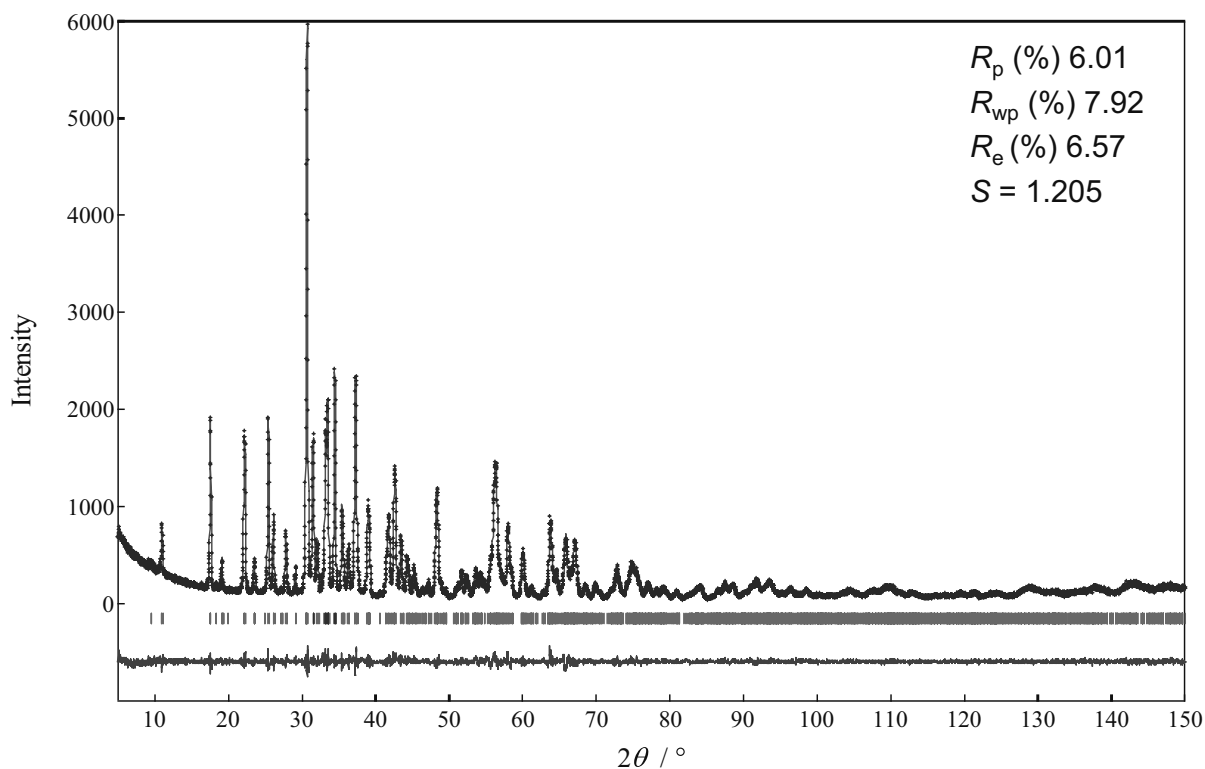
* Step interval (2θ) 10–150°, step 0.02°.

† Abbreviations as in Table 1.

‡ Determined using EMPA. The data of run no. 21 were assumed as the same as those of run no. 22.

§ R_B = R -Bragg factor, R_F = R -structure factor, R_p = R -pattern, R_{wp} = R -weighted pattern, R_e = R -expected, $S(=R_{wp}/R_e)$ = Goodness of fit (Young 1993).|| D-W d = Durbin-Watson d -statistic (Hill and Flack 1987).

Bx = bixbyite, Ep = epidote, Es = esseneite, Hm = hematite, Pm = piemontite.

**FIGURE 1.** Rietveld refinement plot for the product from $q = 0.25$ starting material at 370 MPa and 500 °C (run no. 30). This product was refined with single phase of piemontite. The crosses are the observed data, the solid line is the calculated pattern, and the vertical bars mark all possible Bragg reflections ($\text{CuK}\alpha_1$ and $\text{CuK}\alpha_2$). Bar marks are piemontite. The difference between the observed and calculated patterns is shown at the bottom.

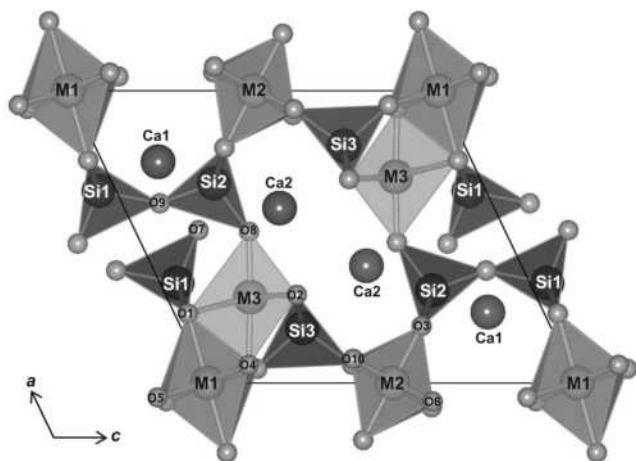


FIGURE 2. Crystal structure of $q = 0.5$ piemontite (run. no. 22) projected down [010] using the program VESTA (Momma and Izumi 2008).

interpreted that the degree of distortion of the M1 octahedra in residual pyroxene decreased during the chemical reaction to form epidote. The peaks F (-0.79 mm/s) and F' (1.93 mm/s) are caused by Fe³⁺ of hematite, because hematite used as starting material showed two peaks at -0.84 and 1.79 mm/s in a range of the Doppler velocity between -4.00 and 4.00 mm/s. The doublet of EE' (IS = 1.16 and QS = 2.37 mm/s) are attributed to Fe²⁺ in epidote or pyroxene.

The Mössbauer spectra of the products from $q = 0.75$ and 0.5 starting materials at 360 and 200 MPa and 500 °C (run nos. 27, 22, and 21 in Table 8) are composed of four doublets of AA', BB', CC', and DD' assigned to Fe³⁺ on M3, Fe³⁺ on M1, and Fe³⁺ in esseneite, respectively (Figs. 3b, 3c, and 3d).

The assignments of the doublets AA', BB', CC', and DD' in the spectra of the products from $q = 0.25$ at 200 MPa (run no. 38) and 370 MPa (run no. 30) (Figs. 3e and 3f) are essentially the same as others. However, there is an additional doublet aa' with IS = 0.36–0.37 and QS = 1.90–1.97 mm/s. In terms of their Mössbauer hyperfine parameters, the doublet aa' is also assigned to Fe³⁺ at M3. The existence of two doublets of Fe³⁺ at M3 (IS = 0.39 and QS = 1.95 mm/s; IS = 0.34 and QS = 2.04 mm/s) has been found for synthetic epidote with $0.5 \leq Fe \leq 0.7$ apfu, which was considered

evidence for the existence of a miscibility gap (Fehr and Heuss-Assbichler 1997). The Fe³⁺ content of Al-Fe³⁺-Mn³⁺ piemontite in run nos. 30 and 38 is 0.12 Fe³⁺ apfu (Table 2). The composition is very different from that of the epidote displaying two Fe³⁺(M3) doublets reported by Fehr and Heuss-Assbichler (1997). These two doublets may imply the existence of an additional miscibility gap at Mn³⁺:Fe³⁺ = 0.75:0.25 bulk composition.

Finally, the site occupancies of Fe³⁺ and Mn³⁺ were determined by combining the results of the chemical analyses, the Rietveld refinement and ⁵⁷Fe Mössbauer analyses, as listed in Table 7.

DISCUSSION

Distributions of Fe³⁺ and Mn³⁺ in the octahedral sites

Generally natural epidote and piemontite contain both Fe³⁺ and Mn³⁺ (Deer et al. 1997; Franz and Liebscher 2004). In most of the previous studies, Fe³⁺ and Mn³⁺ have been assumed to show the same behavior, because the ionic radii of Fe³⁺ [0.645 Å; Shannon (1976)] and Mn³⁺ (0.645 Å) are the same and Fe cannot be distinguished from Mn in X-ray structural analyses. Thus, the ratios of Fe³⁺ and Mn³⁺ at M3 and M1 have been fixed to the Fe_{total}³⁺:Mn_{total}³⁺ ratio. Dollase (1969, 1973) determined Mn³⁺ and Fe³⁺ occupancies in piemontite and epidote, respectively, based on the results of X-ray single-crystal study and ⁵⁷Fe Mössbauer analyses. His results indicated the stronger preference of Fe³⁺ rather than Mn³⁺ for M3. However, as Dollase (1973) pointed out, these results for Mn³⁺ and Fe³⁺ occupancies contradict the theoretical expectation based on the Jahn-Teller effect. Ferraris et al. (1989) carried out a structural refinement of Sr-rich piemontite from St. Marcel (Italy) using the neutron single-crystal diffraction. According to their refinement, Fe³⁺ rather than Mn³⁺ preferred M3. However, it has been interpreted that the substitution of Sr for Ca at A2 promotes incorporation of Mn³⁺ into M1 (Armbruster et al. 2002; Nagashima and Akasaka 2004). The intracrystalline partitioning coefficient (abbreviated as K_D value) for Fe³⁺-Al partitioning, where $K_D = (Fe^{3+}/Al)^{M1}/(Fe^{3+}/Al)^{M3}$, is 0.033–0.054 for epidote synthesized at 0.46–0.55 GPa and 700 °C (0.68–1.00 Fe³⁺ apfu at M1+M3: Giuli et al. 1999), and K_D values for Mn³⁺-Al partitioning, $K_D = (Mn^{3+}/Al)^{M1}/(Mn^{3+}/Al)^{M3}$, are 0.063–0.080 for piemontite synthesized at 1.5 GPa and 800 °C (0.88–1.39 Mn³⁺ apfu at M1+M3: Langer et al. 2002) and 0.038–0.063 for piemontite at 0.2–0.35 GPa and 500

TABLE 7. Cation occupancies at M1, M2, and M3

q^*	1.0	0.75	0.5		0.25	
Synthesis P (MPa)	400	360	200	360	200	370
T (°C)	500	500	500	500	500	500
Run no.	41	27	22	21	38	30
Fe ³⁺	0.91	0.58	0.39	0.39	0.12	0.12
Mn ³⁺	–	0.21	0.53	0.53	0.78	0.73
Total of Fe ³⁺ +Mn ³⁺	0.91	0.79	0.92	0.92	0.90	0.85
Results of Rietveld analysis						
M1	Al0.84Fe0.16(1)	Al0.898Mn0.102(4)	Al0.815Mn0.185(6)	Al0.789Mn0.211(4)	Al0.780Mn0.220(5)	Al0.842Mn0.158(4)
M2	Al1.0	Al1.0	Al1.0	Al1.0	Al1.0	Al1.0
M3	Al0.25Fe0.75	Al0.312Mn0.688	Al0.265Mn0.735	Al0.291Mn0.709	Al0.320Mn0.680	Al0.308Mn0.692
Combined results of Rietveld analysis and Mössbauer spectroscopy						
M1	Al0.84Fe0.16	Al0.90Fe0.08Mn0.02	Al0.81Fe0.06Mn0.13	Al0.79Fe0.08Mn0.13	Al0.78Fe0.01Mn0.21	Al0.84Fe0.01Mn0.15
M2	Al1.00	Al1.00	Al1.00	Al1.00	Al1.00	Al1.00
M3	Al0.25Fe0.75	Al0.31Fe0.50Mn0.19	Al0.27Fe0.33Mn0.40	Al0.29Fe0.31Mn0.40	Al0.32Fe0.11Mn0.57	Al0.31Fe0.11Mn0.58
K_D value						
$[(Fe+Mn)/Al]^{M1}/[(Fe+Mn)/Al]^{M3}$	0.063	0.050	0.087	0.109	0.133	0.086
$(Fe/Mn)^{M1}/(Fe/Mn)^{M3}$		1.520	0.559	0.794	0.247	0.352

* Abbreviations as in Table 1.

TABLE 8. ⁵⁷Fe Mössbauer hyperfine parameters of the run products analyzed by Rietveld method

<i>q</i> *		1.0	0.75	0.5		0.25	
Synthesis <i>P</i> (MPa)		400	360	200	360	200	370
<i>T</i> (°C)		500	500	500	500	500	500
Run no.		41	27	22	21	38	30
Fe ³⁺		0.91	0.58	0.39	0.39	0.12	0.12
Mn ³⁺		–	0.21	0.53	0.53	0.78	0.73
Total of Fe ³⁺ +Mn ³⁺		0.91	0.79	0.92	0.92	0.90	0.85
AA'							
Fe ³⁺ in M3 in epidote	IS (mm/s)	0.357(1)	0.353(1)	0.354(7)	0.350(2)	0.344(3)	0.341(6)
	QS (mm/s)	2.070(2)	2.103(1)	2.11(1)	2.121(4)	2.163(6)	2.22(1)
	FWHH (mm/s)	0.29(4)	0.309(3)	0.294(5)	0.302(6)	0.272(7)	0.25(2)
	Area ratio (%)	62(1)	75(1)	73(1)	66(2)	58(4)	36(6)
aa'							
Fe ³⁺ in M3 in epidote	IS (mm/s)					0.371(8)	0.357(9)
	QS (mm/s)					1.90(2)	1.97(2)
	FWHH (mm/s)					0.24(1)	0.28(2)
	Area ratio (%)					16(2)	35(6)
BB'							
Fe ³⁺ in M1 in epidote	IS (mm/s)	0.336(5)	0.318(4)	0.33(2)	0.355(8)	0.35(1)	0.35(1)
	QS (mm/s)	1.55(1)	1.508(8)	1.57(4)	1.61(2)	1.56(3)	1.51(3)
	FWHH (mm/s)	0.29(4)	0.28(1)	0.28(2)	0.302(6)	0.24(1)	0.28(2)
	Area ratio (%)	13(1)	12.0(6)	13(2)	16(1)	7(1)	9(2)
CC'							
Fe ³⁺ in M1 in esseneite	IS (mm/s)	0.32(1)	0.304(9)	0.31(2)	0.33(1)	0.335(8)	0.32(1)
	QS (mm/s)	0.95(2)	0.90(2)	0.98(5)	0.91(2)	1.09(2)	0.95(2)
	FWHH (mm/s)	0.29(4)	0.28(1)	0.28(2)	0.302(6)	0.24(1)	0.28(2)
	Area ratio (%)	10(1)	8.3(7)	8(2)	12(1)	10(1)	14(2)
DD'							
Fe ³⁺ in M1 in esseneite	IS (mm/s)	0.39(1)	0.37(1)	0.330(1)	0.38(2)	0.343(8)	0.33(3)
	QS (mm/s)	0.53(2)	0.63(3)	0.724(3)	0.48(5)	0.67(2)	0.64(6)
	FWHH (mm/s)	0.29(4)	0.28(1)	0.28(2)	0.302(6)	0.24(1)	0.28(2)
	Area ratio (%)	9(1)	4.6(6)	6(2)	5(1)	8.8(9)	5(2)
EE'							
Fe ²⁺ in epidote or esseneite	IS (mm/s)	1.16(3)					
	QS (mm/s)	2.37(7)					
	FWHH (mm/s)	0.29(4)					
	Area ratio (%)	4.0(3)					
FF'							
Fe ³⁺ in hematite	Peak position of F (mm/s)	–0.79(1)					
	Peak position of F' (mm/s)	1.93(1)					
	FWHH (mm/s)	0.29(4)					
	Area ratio (%)	2.4(4)					
	χ ² /Freedom	1.20	1.34	1.13	1.15	1.10	0.97

Note: Estimated standard deviations are in parentheses (1σ). IS = isomer shift relative to metallic iron absorber, QS = quadrupole splitting, FWHH = full-width at half height. * Abbreviations as in Table 1.

°C (0.46–1.23 Mn³⁺ apfu at M1+M3; Nagashima and Akasaka 2004). The *K_D* value of Mn³⁺ tends to be larger than that of Fe³⁺, i.e., Fe³⁺ rather than Mn³⁺ prefers M3.

As a result of this study, the occupancies of Σ(Fe³⁺+Mn³⁺) in the octahedral sites are plotted collinearly on the regression line of Mn³⁺ occupancies at M3 and M1 of Al-Mn³⁺ binary piemontite series by Nagashima and Akasaka (2004) (Fig. 4). Fe³⁺ occupancies in the synthetic Al-Fe³⁺ binary epidote series by Giuli et al. (1999) are also similar to those of Σ(Fe³⁺+Mn³⁺) and Mn³⁺. Moreover, the range of the *K_D* values of Σ(Fe³⁺+Mn³⁺) (*K_D* = [(Fe³⁺ + Mn³⁺)/Al]^{M1}/[(Fe³⁺ + Mn³⁺)/Al]^{M3}) in this study is almost overlapping with those of Fe³⁺ in Al-Fe³⁺ epidote (Giuli et al. 1999) and Mn³⁺ in Al-Mn³⁺ piemontite (Langer et al. 2002; Nagashima and Akasaka 2004) (Fig. 5). It is also shown that the *K_D* values tend to increase with increasing Mn content in the synthetic phases.

In spite of the quite similar *K_D* values of Σ(Fe³⁺+Mn³⁺) vs. Al, intracrystalline partitioning coefficients of individual Fe³⁺ vs. Mn³⁺ between M3 and M1 are different. The *K_D* value of Fe³⁺ vs. Mn³⁺ [*K_D* = (Fe³⁺/Mn³⁺)^{M1}/(Fe³⁺/Mn³⁺)^{M3}] increases with increasing Fe content. In the case of epidote from run no. 27 (0.58 Fe³⁺ + 0.21 Mn³⁺), the *K_D* value of Fe³⁺ vs. Mn³⁺ is 1.52, indicating

that Fe³⁺ prefers M1, whereas in epidote/piemontite with Fe³⁺ content less than Mn³⁺, i.e., piemontite from run nos. 22, 21, 38, and 30, the *K_D* values are 0.25–0.79 indicating a stronger Mn³⁺ rather than Fe³⁺ preference for M1. These results indicate that Fe³⁺ and Mn³⁺ distribute among octahedral sites according to their individual distribution schemes by the substitutions of Fe³⁺ ↔ Al and Mn³⁺ ↔ Al, respectively. Taking into account the almost identical ionic radii of Fe³⁺ and Mn³⁺, our result may be generalized that the cations of transition elements having similar ionic radii are distributed among octahedral sites based on individual preference, such as Fe³⁺ ↔ Al and Mn³⁺ ↔ Al. Figure 6 shows the relationship between Fe or Mn content (apfu) at M3 against that at M1. The increase of Mn³⁺ content at M1 is about 1.5× larger than that of Fe³⁺. It indicates that Mn³⁺ has a stronger preference for M1 than Fe³⁺ at this temperature. This result agrees with the relation between *K_D* value of Mn³⁺ in Al-Mn³⁺ piemontite and that of Fe³⁺ in Al-Fe³⁺ epidote.

Nagashima and Akasaka (2004) discussed the pressure and temperature dependence on the *K_D* values and Al/Mn³⁺ partitioning, and concluded that the distribution of Mn³⁺ at M3 and M1 is not significantly influenced by the crystallization pressure and temperature. On the basis of their result, we consider that

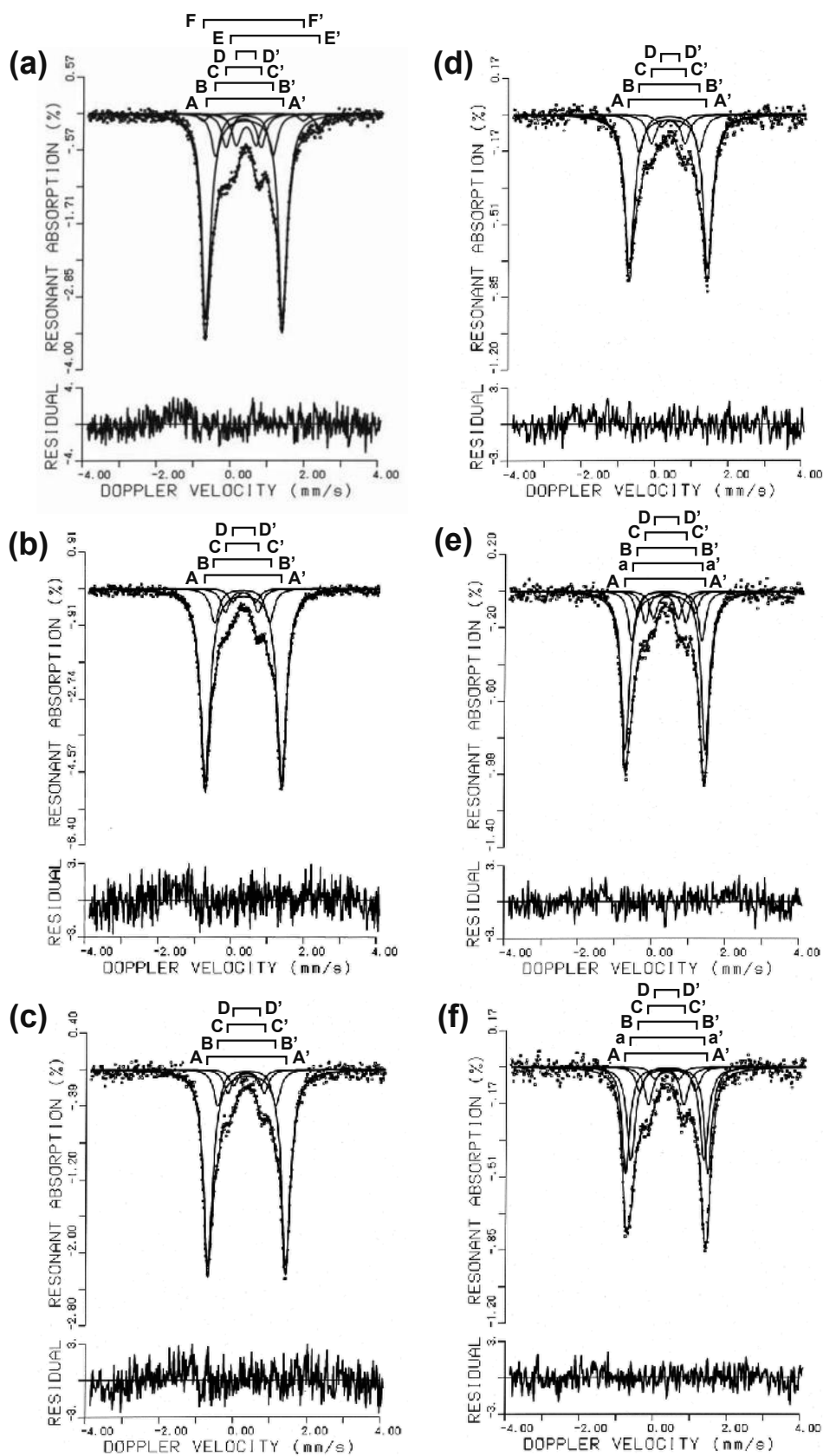


FIGURE 3. ⁵⁷Fe Mössbauer spectra of Al-Fe³⁺ and Al-Fe³⁺-Mn³⁺ series synthetic epidote and piemontite at 293 K. (a) Run no. 41 ($q = 1.0$), (b) run no. 27 ($q = 0.75$), (c) run no. 22 ($q = 0.5$), (d) run no. 21 ($q = 0.5$), (e) run no. 38 ($q = 0.25$), and (f) run no. 30 ($q = 0.25$). The refined Mössbauer hyperfine parameters are listed in Table 8.

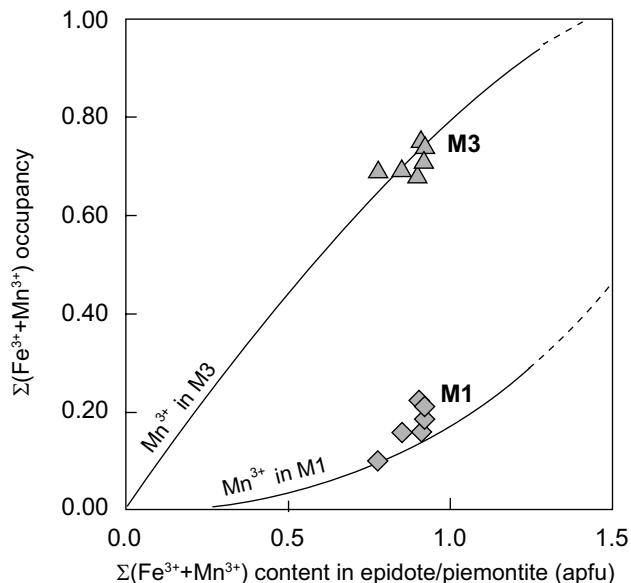


FIGURE 4. Variations of the $\Sigma(\text{Fe}^{3+}+\text{Mn}^{3+})$ occupancies of the M1 and M3 sites against $\Sigma(\text{Fe}^{3+}+\text{Mn}^{3+})$ contents in synthetic epidote and piemontite. Gray diamonds and gray triangles represent the $\Sigma(\text{Fe}^{3+}+\text{Mn}^{3+})$ occupancies at M1 and M3, respectively. The lines show the regression curves of Mn^{3+} occupancies at M3 and M1 of synthetic Al-Mn³⁺ series piemontite determined by Nagashima and Akasaka (2004). All symbols are larger than 1 σ error bars.

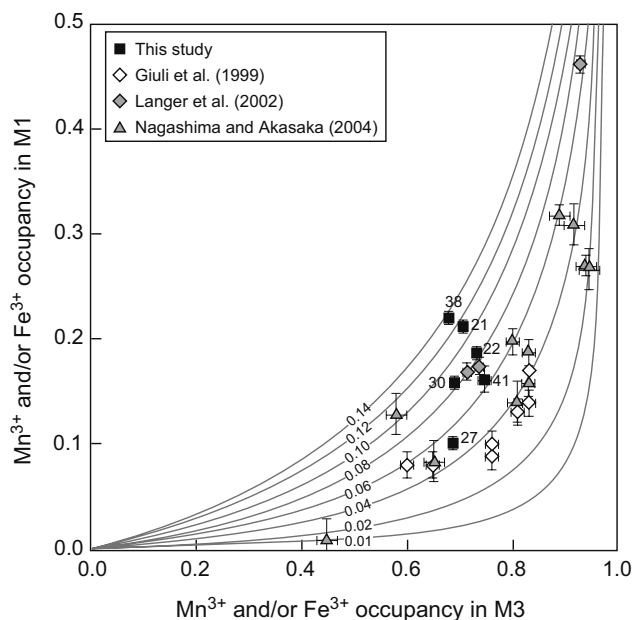


FIGURE 5. Mn³⁺ and/or Fe³⁺ occupancy in M1 vs. M3 [$K_D(\text{Mn}^{3+}) = (\text{Mn}^{3+}/\text{Al})_{\text{M1}}/(\text{Mn}^{3+}/\text{Al})_{\text{M3}}$, $K_D(\text{Fe}^{3+}) = (\text{Fe}^{3+}/\text{Al})_{\text{M1}}/(\text{Fe}^{3+}/\text{Al})_{\text{M3}}$, and $K_D[\Sigma(\text{Fe}^{3+} + \text{Mn}^{3+})] = [(\text{Fe}^{3+} + \text{Mn}^{3+})/\text{Al}]_{\text{M1}}/[(\text{Fe}^{3+} + \text{Mn}^{3+})/\text{Al}]_{\text{M3}}$. Ideal fractionation K_D values of 0.01, 0.02, 0.04, 0.06, 0.08, 0.10, 0.12, and 0.14 are shown. The 1 σ error bars are represented (some are smaller than the symbol).

the pressure and temperature dependence on the K_D values and $\text{Fe}^{3+}/\text{Mn}^{3+}$ partitioning would be negligible, although the pressure or temperature dependence of Al/Fe³⁺ or Fe³⁺/Mn³⁺ partitioning have not been studied systematically.

Structural changes caused by cation substitutions in the octahedral sites

The structural variations of synthetic Al-Mn³⁺ piemontite were investigated by Nagashima and Akasaka (2004). They concluded that non-linear variations of the unit-cell parameters are due to the Jahn-Teller effect. The characteristic variation of the a -axis was confirmed. The a -axis decreases with increasing Mn³⁺ content up to 1 apfu, and it starts increasing with increasing Mn³⁺ > 1 apfu. On the other hand, the a -, b -, c -axes of synthetic Al-Fe³⁺ epidote simply increase with increasing Fe³⁺ content (Giuli et al. 1999). In the case that each pure Al-Fe³⁺ epidote and Al-Mn³⁺ piemontite has the same Fe³⁺ and Mn³⁺ concentrations, the b -axis of epidote is shorter than that of piemontite (Giuli et al. 1999; Langer et al. 2002; Nagashima and Akasaka 2004). The variation of the unit-cell parameters with M³⁺ in this study is not simple. It shows the combined result of linear variation due to Al \leftrightarrow Fe³⁺ substitution (Giuli et al. 1999) and nonlinear variation due to Al \leftrightarrow Mn³⁺ substitution (Nagashima and Akasaka 2004). The a -axis decreases with the increasing Mn³⁺ content as found for Al-Mn³⁺ piemontite, but the b -axis behaves in the opposite way (Fig. 7). Moreover, in the present study, the QS values of Fe³⁺ at M3 (AA') increase from 2.07 to 2.22 mm/s with increasing Mn³⁺ at M3 (Table 8). This indicates an increase of the site distortion of M3O₆ octahedra with increasing Mn³⁺ content at M3. However, the variations of the unit-cell parameters and distortion parameters with Fe³⁺ \leftrightarrow Mn³⁺ substitution are not distinct. Bermanec et al. (1994) suggested that the high octahedral Mn³⁺

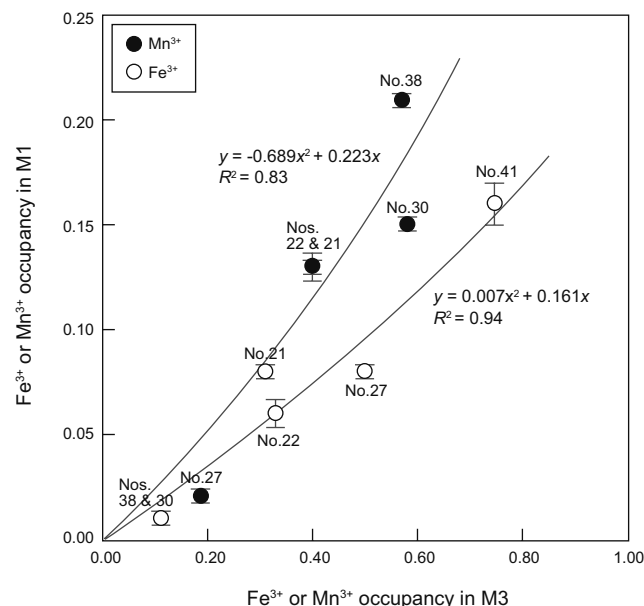


FIGURE 6. Relationship between Fe³⁺ or Mn³⁺ content in M3 and M1. The 1 σ error bars are represented. However, all symbols are larger than 1 σ error bars in X direction.

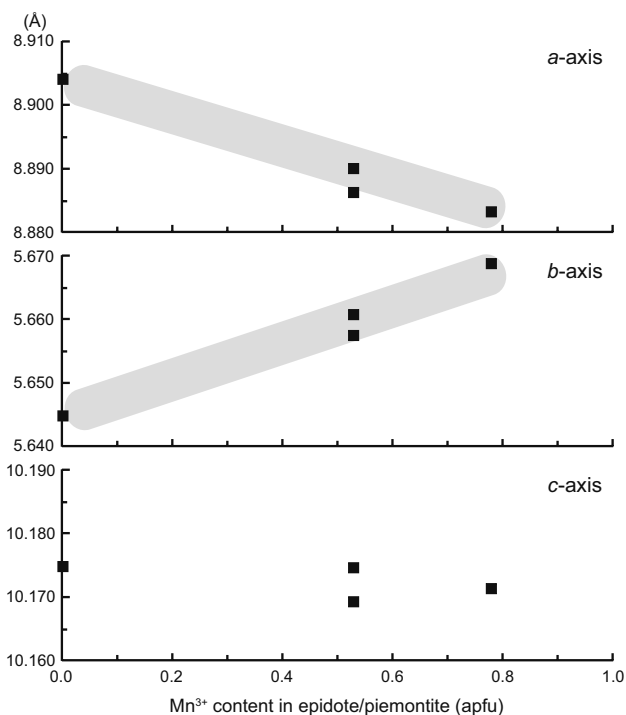


FIGURE 7. Variations of the unit-cell parameters vs. Mn³⁺ content (apfu) of the synthetic epidote/piemontite in this study. Data, with ca. 0.9 $\Sigma(\text{Fe}^{3+} + \text{Mn}^{3+})$ apfu, are plotted. All symbols are larger than 1 σ error bars.

content in piemontite does not necessarily show stronger deformation due to Jahn-Teller distortion than epidote and clinozoisite, and Ferraris et al. (1989) also argued that the distortion of MO₆ octahedra tends to be independent from the Mn³⁺ content of these sites. In the case that both Mn³⁺ and Fe³⁺ occur in epidote-group minerals, it is very difficult to evaluate the contribution of the Jahn-Teller effect on the crystal structure. However, the results of this study clarify that the Jahn-Teller effect acts on the crystal structure, but has no clear effect on the site distribution.

ACKNOWLEDGMENTS

We thank Fujio Izumi at National Institute for Materials Science (NIMS) for his permission to use the Rietan-2000 program, Thomas Armbruster at University of Bern for his constructive comments on this manuscript, and Barry Roser at Shimane University for his critical reading of this manuscript. We also thank associate editor M.D. Dyar, and D. Malczewski and A. Liebscher for their constructive comments on this manuscript.

REFERENCES CITED

Akasaka, M. (1983) ⁵⁷Fe Mössbauer study of clinopyroxene in the join CaFe³⁺AlSiO₆-CaTiAl₂O₆. *Physics and Chemistry of Minerals*, 9, 205–211.

— (1990) Clinopyroxene on the join CaMgSi₂O₆-CaFe³⁺AlSiO₆-CaTiAl₂O₆ at low oxygen fugacity. *Proceedings of the Indian Academy of Sciences (Earth and Planetary Sciences)*, 99, 39–48.

Akasaka, M. and Shinno, I. (1992) Mössbauer spectroscopy and its recent application to silicate mineralogy. *Journal of Mineralogical Society of Japan*, 21, 3–20 (in Japanese with English abstract).

Anastasiou, P. and Langer, K. (1977) Synthesis and physical properties of piemontite Ca₂Al_{3-p}Mn_p³⁺(Si₂O₇/SiO₄/O/OH). *Contributions to Mineralogy and Petrology*, 60, 225–245.

Armbruster, T., Gnos, E., Dixon, R., Gutzmer, J., Hejny, C., Döbelin, N., and Medenbach, O. (2002) Manganvesuvianite and tweddillite, two new Mn³⁺-silicate minerals from the Kalahari manganese fields, South Africa. *Mineralogical Magazine*, 66, 137–150.

Bermanec, V., Armbruster, T., Oberhänsli, R., and Zebec, V. (1994) Crystal chemis-

try of Pb- and REE-rich piemontite from Nezilovo, Macedonia. *Schweizerische Mineralogische und Petrographische Mitteilungen*, 74, 321–328.

Bish, D.L. and Reynolds, R.C. (1989) Sample preparation for X-ray diffraction. In D.L. Bish and J.E. Post, Eds., *Modern Powder Diffraction*, 20, p. 73–99. Reviews in Mineralogy, Mineralogical Society of America, Chantilly, Virginia.

Blacke, R.Z., Hessevick, R.E., Zoltai, T., and Finger, L.W. (1966) Refinement of the hematite structure. *American Mineralogist*, 51, 123–129.

Bonazzi, P. and Menchetti, S. (1994) Structural variations induced by heat treatment in allanite and REE-bearing piemontite. *American Mineralogist*, 79, 1176–1184.

— (1995) Monoclinic members of the epidote group: Effects of the Al³⁺↔Fe³⁺↔Fe²⁺ substitution and of the entry of REE³⁺. *Mineralogy and Petrology*, 53, 133–153.

Bonazzi, P., Menchetti, S., and Palenzona, A. (1990) Strontioepimontite, a new member of the epidote group from Val Graveglia, Liguria, Italy. *European Journal of Mineralogy*, 2, 519–523.

Bonazzi, P., Garbarino, C., and Menchetti, S. (1992) Crystal chemistry of piemontites: REE-bearing piemontite from Monte Brugiana, Alpi Apuane, Italy. *European Journal of Mineralogy*, 4, 23–33.

Burns, R.G. and Strens, R.G.J. (1967) Structural interpretation of polarized absorption spectra of the Al-Fe-Mn-Cr epidotes. *Mineralogical Magazine*, 36, 204–226.

Cosca, M.A. and Peacor, D.R. (1987) Chemistry and structure of esseneite (CaFe²⁺AlSiO₆), a new pyroxene produced by pyrometamorphism. *American Mineralogist*, 72, 148–156.

Deer, W.A., Howie, R.A., and Zussman, J. (1997) *Rock-forming minerals. IB (Second edition), Disilicates and ring silicates*, p. 629. Geological Society Publishing House, U.K.

Dollase, W.A. (1968) Refinement and comparison of the structures of zoisite and clinozoisite. *American Mineralogist*, 53, 1882–1898.

— (1969) Crystal structure and cation ordering of piemontite. *American Mineralogist*, 54, 710–717.

— (1971) Refinement of the crystal structures of epidote, allanite, and Hancockite. *American Mineralogist*, 56, 447–464.

— (1973) Mössbauer spectra and iron distribution in the epidote-group minerals. *Zeitschrift für Kristallographie*, 138, 41–63.

— (1986) Correction of intensities for preferred orientation in powder diffractometry: Application of the March model. *Journal of Applied Crystallography*, 19, 267–272.

Fehr, K.T. and Heuss-Assbichler, S. (1997) Intracrystalline equilibria and immiscibility along the join clinozoisite-epidote: An experimental and ⁵⁷Fe Mössbauer study. *Neues Jahrbuch für Mineralogie Abhandlungen*, 172, 43–67.

Ferraris, G., Ivaldi, G., Fuess, H., and Gregson, D. (1989) Manganese/iron distribution in a strontian piemontite by neutron diffraction. *Zeitschrift für Kristallographie*, 187, 145–151.

Franz, G. and Liebscher, A. (2004) Physical and chemical properties of the epidote minerals: An introduction. In A. Liebscher and G. Franz, Eds., *Epidotes*, 56, p. 1–81. Reviews in Mineralogy and Geochemistry, Mineralogical Society of America, Chantilly, Virginia.

Frenzel, V.G., Nuber, B., and Ottemann, J. (1985) Kristallchemische Untersuchungen an Ferridiopsiden des Katzenbuckels (Odenwald, BRD). *Chemie der Erde*, 44, 299–309.

Fukushima, H., Minakawa, T., and Nishio, D. (2005) Ba-rich tweddillite from the Kamisugai mine in the Smabagawa metamorphic belt, Shikoku, Japan. *Japanese Magazine of Mineralogical and Petrological Sciences*, 34, 69–76 (in Japanese with English abstract).

Geller, S. (1971) Structures of α-Mn₂O₃ (Mn_{0.983}Fe_{0.017})₂O₃ and (Mn_{0.37}Fe_{0.63})₂O₃ and relation to magnetic ordering. *Acta Crystallographica*, B27, 821–828.

Giuli, G., Bonazzi, P., and Menchetti, S. (1999) Al-Fe disorder in synthetic epidotes: A single-crystal X-ray diffraction study. *American Mineralogist*, 84, 933–936.

Hill, R.J. and Flack, H.D. (1987) The use of the Durbin-Watson *d* statistic in Rietveld analysis. *Journal of Applied Crystallography*, 20, 356–361.

Ito, T., Morimoto, N., and Sadanaga, R. (1954) On the structure of epidote. *Acta Crystallographica*, 7, 53–59.

Izumi, F. (1993) Rietveld analysis program RIETAN and PREMOS and special applications. In R.A. Young, Ed., *The Rietveld Method*, p. 236–253. Oxford Science Publications, U.K.

Izumi, F. and Ikeda, T. (2000) A Rietveld analysis program RIETAN-98 and its application to zeolites. *Material Science Forum*, 321–324.

Kvick, A., Pluth, J.J., Richardson, J.W., and Smith, J.V. (1988) The ferric ion distribution and hydrogen bonding in epidote: A neutron diffraction study at 15 K. *Acta Crystallographica*, B44, 351–355.

Langer, K., Tillmanns, E., Kersten, M., Almen, H., and Armi, R.K. (2002) The crystal chemistry of Mn³⁺ in the clino- and orthoepidote structure types, Ca₂M₃³⁺(OH/O/SiO₄/Si₂O₇): A structural and spectroscopic study of some natural piemontites and “thulites” and their synthetic equivalents. *Zeitschrift für Kristallographie*, 217, 1–18.

Liebscher, A. (2004) Spectroscopy of epidote minerals. In A. Liebscher and G.

- Franz, Eds., *Epidotes*, 56, p. 125–170. Reviews in Mineralogy and Geochemistry, Mineralogical Society of America, Chantilly, Virginia.
- Liou, J.G. (1973) Synthesis and stability relations of epidote, Ca₂Al₂FeSi₃O₁₂(OH). *Journal of Petrology*, 14, 381–413.
- Matsui, Y., Shono, Y., and Maeda, Y. (1972) Mössbauer spectra of synthetic and natural calcium-rich clinopyroxenes. *Mineralogical Journal*, 7, 88–107.
- Momma, K. and Izumi, F. (2008) VESTA: A three-dimensional visualization system for electronic and structural analysis. *Journal of Applied Crystallography*, 41, 653–658.
- Nagashima, M. (2006) Hydrothermal syntheses of epidote and piemontites on the join Ca₂Al₃Fe³⁺Si₃O₁₂(OH)-Ca₂Al₂Mn³⁺Si₃O₁₂(OH) at relatively low pressures of 200–400 MPa. *Journal of Mineralogical and Petrological Sciences*, 101, 1–9.
- Nagashima, M. and Akasaka, M. (2004) An X-ray Rietveld study of piemontite on the join Ca₂Al₃Si₃O₁₂(OH)-Ca₂Mn³⁺Si₃O₁₂(OH) formed by hydrothermal synthesis. *American Mineralogist*, 89, 1119–1129.
- Nagashima, M., Geiger, C.A., and Akasaka, M. (2009) A crystal-chemical investigation of clinozoisite synthesized along the join Ca₂Al₃Si₃O₁₂(OH)-Ca₂Al₃CrSi₃O₁₂(OH). *American Mineralogist*, 94, 1351–1360.
- Paesano, A., Kunrath, J.I., and Vasquez, A. (1983) A ⁵⁷Fe Mössbauer study of epidote. *Hyperfine Interactions*, 15/16, 841–844.
- Post, J.E. and Bish, D.L. (1989) Rietveld refinement of crystal structures using powder X-ray diffraction data. In D.L. Bish and J.E. Post, Eds., *Modern Powder Diffraction*, 20, p. 277–308. Reviews in Mineralogy, Mineralogical Society of America, Chantilly, Virginia.
- Raudsepp, M., Hawthorne, F.C., and Turnock, A.C. (1990) Evaluation of the Rietveld method for the characterization of fine-grained products of mineral synthesis: The diopside–hedenbergite join. *Canadian Mineralogist*, 28, 93–109.
- Shannon, R.D. (1976) Revised effective ionic radii and systematic studies of interatomic distances in halides and chalcogenides. *Acta Crystallographica*, A32, 751–767.
- Taran, M.N. and Langer, K. (2000) Electronic absorption spectra of Fe³⁺ in andradite and epidote at different temperatures and pressures. *European Journal of Mineralogy*, 12, 7–15.
- Toraya, H. (1990) Array-type universal profile function for powder pattern fitting. *Journal of Applied Crystallography*, 23, 485–491.
- Young, R.A. (1993) Introduction to the Rietveld method. In R.A. Young, Ed., *The Rietveld Method*, p. 1–38. Oxford, U.K.

MANUSCRIPT RECEIVED OCTOBER 9, 2009

MANUSCRIPT ACCEPTED MARCH 24, 2010

MANUSCRIPT HANDLED BY M. DARBY DYAR

Table 4. Refined atomic positions

q^*				1.0		0.75		0.5		0.25	
Ato	neq	W_{\ddagger}^{\dagger}	$x,y,$	400 MPa	360 MPa	200 MPa	360 MPa	200 MPa	370 MPa		
m	\dagger		z	500 °C	500 °C						
				Run	Run	Run	Run	Run	Run	Run	
				no.41	no.27	no.22	no.21	no.38	no.30		
Fe ³⁺				0.91	0.58	0.39	0.39	0.12	0.12		
Mn ³⁺				-	0.21	0.53	0.53	0.78	0.73		
Total of Fe ³⁺ +Mn ³⁺				0.91	0.79	0.92	0.92	0.90	0.85		
O1	4	<i>f</i>	<i>x</i>	0.235(1)	0.2311(7)	0.2376(4)	0.2373(8)	0.2313(9)	0.2328(7)		
			<i>y</i>	0.993(2)	0.988(1)	0.984(1)	0.985(1)	0.983(1)	0.992(1)		
			<i>z</i>	0.041(1)	0.0362(7)	0.0363(9)	0.0349(7)	0.0329(8)	0.0346(6)		
O2	4	<i>f</i>	<i>x</i>	0.305(1)	0.3077(7)	0.302(1)	0.3062(9)	0.3097(9)	0.3061(7)		
			<i>y</i>	0.977(2)	0.978(1)	0.982(2)	0.981(1)	0.981(1)	0.9794(9)		
			<i>z</i>	0.355(1)	0.3570(8)	0.355(1)	0.3566(8)	0.362(1)	0.3433(6)		
O3	4	<i>f</i>	<i>x</i>	0.798(1)	0.8011(8)	0.805(1)	0.8018(9)	0.796(1)	0.7982(8)		
			<i>y</i>	0.015(2)	0.019(1)	0.017(1)	0.018(1)	0.016(1)	0.019(1)		
			<i>z</i>	0.342(1)	0.3476(7)	0.3479(9)	0.3487(8)	0.3449(9)	0.3433(6)		
O4	2	<i>e</i>	<i>x</i>	0.052(2)	0.055(1)	0.062(1)	0.062(1)	0.066(1)	0.062(1)		
			<i>y</i>	1/4	1/4	1/4	1/4	1/4	1/4		
			<i>z</i>	0.129(2)	0.140(1)	0.135(2)	0.1369(2)	0.133(1)	0.137(1)		
O5	2	<i>e</i>	<i>x</i>	0.036(2)	0.0379(8)	0.049(1)	0.0464(9)	0.042(1)	0.041(1)		
			<i>y</i>	3/4	3/4	3/4	3/4	3/4	3/4		
			<i>z</i>	0.151(2)	0.1464(7)	0.153(1)	0.1480(6)	0.153(1)	0.148(1)		
O6	2	<i>e</i>	<i>x</i>	0.062(2)	0.0535(7)	0.063(1)	0.0612(8)	0.062(1)	0.064(1)		
			<i>y</i>	3/4	3/4	3/4	3/4	3/4	3/4		
			<i>z</i>	0.411(2)	0.402(1)	0.415(1)	0.408(1)	0.409(1)	0.408(1)		
O7	2	<i>e</i>	<i>x</i>	0.516(2)	0.5207(7)	0.523(2)	0.5182(9)	0.522(1)	0.514(1)		
			<i>y</i>	3/4	3/4	3/4	3/4	3/4	3/4		
			<i>z</i>	0.173(2)	0.1782(7)	0.172(1)	0.1773(7)	0.182(1)	0.1793(9)		
O8	2	<i>e</i>	<i>x</i>	0.524(2)	0.5222(8)	0.518(2)	0.5182(9)	0.525(1)	0.523(1)		
			<i>y</i>	1/4	1/4	1/4	1/4	1/4	1/4		
			<i>z</i>	0.309(2)	0.3076(9)	0.307(1)	0.301(1)	0.303(1)	0.3100(9)		
O9	2	<i>e</i>	<i>x</i>	0.646(2)	0.622(1)	0.615(1)	0.619(1)	0.622(1)	0.622(1)		
			<i>y</i>	1/4	1/4	1/4	1/4	1/4	1/4		
			<i>z</i>	0.104(2)	0.098(1)	0.102(1)	0.098(1)	0.100(1)	0.0975(9)		
O10	2	<i>e</i>	<i>x</i>	0.071(2)	0.076(1)	0.083(2)	0.079(1)	0.075(1)	0.083(1)		
			<i>y</i>	1/4	1/4	1/4	1/4	1/4	1/4		
			<i>z</i>	0.425(2)	0.429(1)	0.425(1)	0.428(1)	0.417(1)	0.4308(9)		
Ca1	2	<i>e</i>	<i>x</i>	0.7528(6)	0.7541(4)	0.7571(6)	0.7539(4)	0.7558(5)	0.7554(4)		
			<i>y</i>	3/4	3/4	3/4	3/4	3/4	3/4		
			<i>z</i>	0.1498(7)	0.1498(4)	0.1508(6)	0.1492(4)	0.1547(5)	0.1520(4)		
Ca2	2	<i>e</i>	<i>x</i>	0.6092(7)	0.6057(4)	0.5988(6)	0.6000(5)	0.5993(5)	0.6006(5)		
			<i>y</i>	3/4	3/4	3/4	3/4	3/4	3/4		
			<i>z</i>	0.4222(6)	0.4247(4)	0.4197(5)	0.4229(4)	0.4212(4)	0.4233(3)		

M1	2	<i>a</i>	<i>x</i>	0	0	0	0	0	0
			<i>y</i>	0	0	0	0	0	0
			<i>z</i>	0	0	0	0	0	0
M2	2	<i>c</i>	<i>x</i>	0	0	0	0	0	0
			<i>y</i>	0	0	0	0	0	0
			<i>z</i>	1/2	1/2	1/2	1/2	1/2	1/2
M3	2	<i>e</i>	<i>x</i>	0.2959(5)	0.2948(4)	0.2941(5)	0.2955(4)	0.3002(5)	0.2983(4)
			<i>y</i>	1/4	1/4	1/4	1/4	1/4	1/4
			<i>z</i>	0.2262(5)	0.2245(3)	0.2263(4)	0.2261(4)	0.2253(4)	0.2240(3)
Si1	2	<i>e</i>	<i>x</i>	0.3380(9)	0.3399(5)	0.3431(7)	0.3401(6)	0.3408(7)	0.3374(5)
			<i>y</i>	3/4	3/4	3/4	3/4	3/4	3/4
			<i>z</i>	0.0461(7)	0.0475(4)	0.0475(6)	0.0469(5)	0.0469(6)	0.0460(4)
Si2	2	<i>e</i>	<i>x</i>	0.6814(9)	0.6812(6)	0.6831(8)	0.6828(7)	0.6867(8)	0.6847(5)
			<i>y</i>	1/4	1/4	1/4	1/4	1/4	1/4
			<i>z</i>	0.2766(9)	0.2726(5)	0.2734(7)	0.2750(5)	0.2784(6)	0.2748(4)
Si3	2	<i>e</i>	<i>x</i>	0.1885(9)	0.1873(5)	0.1881(7)	0.1871(6)	0.1879(6)	0.1872(5)
			<i>y</i>	3/4	3/4	3/4	3/4	3/4	3/4
			<i>z</i>	0.324(1)	0.3225(5)	0.3267(8)	0.3245(6)	0.3226(7)	0.3218(5)

TABLE 5. Interatomic distances (Å)

<i>q</i> *		1.0	0.75	0.5		0.25	
Synthesis <i>P</i> (MPa)		400	360	200	360	200	370
<i>T</i> (°C)		500	500	500	500	500	500
Run no.		41	27	22	21	38	30
Fe ³⁺		0.91	0.58	0.39	0.39	0.12	0.12
Mn ³⁺		-	0.21	0.53	0.53	0.78	0.73
Total of Fe ³⁺ +Mn ³⁺		0.91	0.79	0.92	0.92	0.90	0.85
Ca1-O1	×2	2.46(1)	2.455(7)	2.441(9)	2.427(7)	2.476(8)	2.435(6)
)))))
-O3	×2	2.35(1)	2.410(7)	2.396(9)	2.422(8)	2.356(9)	2.370(6)
)))))
-O5		2.51(1)	2.541(8)	2.58(1)	2.605(8)	2.55(1)	2.556(8)
)))))
-O6		2.89(1)	2.797(9)	2.89(1)	2.867(9)	2.84(1)	2.856(8)
)))))
-O7		2.22(1)	2.216(8)	2.18(1)	2.234(9)	2.21(1)	2.272(9)
)))))
Average		2.46	2.469	2.47	2.486	2.47	2.471
-O9	×2	2.946(4)	3.022(3)	3.048(4)	3.031(3)	3.031(3)	3.030(3)
)))))
Average		2.57	2.592	2.60	2.607	2.59	2.595
Ca2-O2	×2	2.80(1)	2.757(7)	2.759(9)	2.733(8)	2.713(8)	2.727(6)
)))))
-O2'	×2	2.57(1)	2.533(8)	2.57(1)	2.539(8)	2.51(1)	2.556(6)
)))))
-O3	×2	2.62(1)	2.667(7)	2.71(1)	2.693(8)	2.663(9)	2.699(6)

-O7		2.30(2)	2.287(8)	2.31(1)	2.283(7)	2.23(1)	2.260(8)
))))))
-O10		2.59(1)	2.574(9)	2.58(1)	2.59(1)	2.64(1)	2.548(8)
))))))
Average		2.61	2.597	2.62	2.600	2.58	2.597
-O8	×2	3.015(6)	3.035(3)	3.019(5)	3.049(4)	3.038(4)	3.025(3)
))))))
Average		2.69	2.685	2.70	2.69	2.67	2.682
M1-O1	×2	1.95(1)	1.926(6)	1.98(1)	1.985(7)	1.937(7)	1.941(6)
))))))
-O4	×2	1.85(1)	1.915(7)	1.88(1)	1.894(8)	1.869(8)	1.897(6)
))))))
-O5	×2	2.00(1)	1.975(7)	2.00(1)	1.977(8)	2.014(9)	1.982(6)
))))))
Average		1.93	1.939	1.95	1.953	1.940	1.940
M2-O3	×2	1.83(1)	1.788(7)	1.758(8)	1.776(7)	1.824(8)	1.817(6)
))))))
-O6	×2	1.88(1)	1.904(5)	1.86(1)	1.900(5)	1.897(9)	1.912(7)
))))))
-O10	×2	1.84(1)	1.847(7)	1.90(1)	1.866(7)	1.913(9)	1.870(6)
))))))
Average		1.85	1.846	1.84	1.847	1.878	1.866
M3-O1	×2	2.25(1)	2.293(6)	2.328(8)	2.333(6)	2.337(8)	2.287(5)
))))))
-O2	×2	2.00(1)	2.014(7)	1.98(1)	1.997(7)	2.042(8)	2.011(6)
))))))
-O4		1.96(1)	1.925(8)	1.86(1)	1.874(8)	1.88(1)	1.891(9)
))))))
-O8		1.83(2)	1.827(7)	1.80(1)	1.80(1)	1.81(1)	1.802(8)
))))))
Average		2.05	2.061	2.05	2.056	2.075	2.048
Si1-O1	×2	1.638(9)	1.633(6)	1.60(1)	1.588(6)	1.610(7)	1.630(5)
))))))
-O7		1.55(1)	1.58(1)	1.55(1)	1.57(1)	1.61(1)	1.572(8)
))))))
-O9		1.59(2)	1.658(9)	1.71(1)	1.66(1)	1.66(1)	1.648(8)
))))))
Average		1.60	1.62	1.62	1.60	1.62	1.620
Si2-O3	×2	1.63(1)	1.651(7)	1.667(8)	1.650(7)	1.611(8)	1.617(6)
))))))
-O8		1.57(2)	1.60(1)	1.64(1)	1.59(1)	1.56(1)	1.62(1)
-O9		1.65(2)	1.62(1)	1.58(1)	1.64(1)	1.66(1)	1.642(8)
))))))
Average		1.62	1.63	1.64	1.63	1.61	1.624
Si3-O2	×2	1.591(9)	1.619(6)	1.603(9)	1.623(7)	1.634(8)	1.616(5)

-O5))))))
	1.70(2)	1.71(1)	1.67(1)	1.69(1)	1.66(1)	1.684(9)
-O6	1.70(2)	1.70(1)	1.70(1)	1.67(1)	1.70(1)	1.67(1)
Average	1.65	1.66	1.64	1.65	1.66	1.647

* Abbreviations as in Table 1.

Table 6. Selected interatomic angles (°)

q^*	1.0	0.75	0.5	0.25		
Synthesis P (MPa)	400	360	200	360	200	370
T (°C)	500	500	500	500	500	500
Run no.	41	27	22	21	38	30
Fe ³⁺	0.91	0.58	0.39	0.39	0.12	0.12
Mn ³⁺	-	0.21	0.53	0.53	0.78	0.73
Total of Fe ³⁺ +Mn ³⁺	0.91	0.79	0.92	0.92	0.90	0.85
O1-M1-O4	86.9(5)	88.4(3)	86.7(4)	87.1(3)	86.2(4)	86.2(3)
O1-M1-O5	88.9(4)	89.6(3)	92.0(4)	91.4(3)	90.0(4)	89.5(3)
O4-M1-O5	94.7(5)	93.5(3)	93.9(3)	94.3(1)	94.6(3)	94.4(2)
O3-M2-O6	89.7(5)	88.1(3)	90.7(4)	90.2(3)	90.2(4)	90.2(3)
O3-M2-O10	91.0(5)	89.7(3)	89.5(5)	89.1(4)	90.7(4)	88.6(3)
O6-M2-O10	98.6(5)	98.4(3)	97.6(3)	97.7(2)	96.2(3)	97.5(3)
O1-M3-O1'	80.1(5)	80.6(3)	80.6(4)	80.1(3)	80.7(4)	79.7(3)
O1-M3-O2	88.9(4)	89.3(3)	89.1(3)	89.7(2)	90.3(3)	89.5(2)
O1-M3-O4	76.3(5)	78.36(3)	77.8(1)	78.1(2)	75.3(3)	77.2(3)
O1-M3-O8	101.9(5)	102.3(2)	100.3(4)	99.4(3)	102.1(3)	103.7(2)
O2-M3-O2'	100.6(6)	99.4(4)	99.9(5)	99.5(4)	96.8(5)	99.5(3)
O2-M3-O4	93.0(4)	92.0(3)	92.7(3)	92.8(2)	93.1(4)	91.4(3)
O2-M3-O8	88.5(4)	87.6(2)	89.0(3)	89.4(3)	89.3(3)	87.9(2)
O1-Si1-O1'	113.7(9)	110.7(6)	111.8(6)	113.7(7)	110.3(7)	114.3(5)
O1-Si1-O7	112.5(5)	114.7(3)	115.2(4)	113.8(3)	115.0(4)	112.9(3)
O1-Si1-O9	104.3(5)	106.4(3)	106.3(4)	105.7(3)	105.5(4)	105.8(3)
O7-Si1-O9	108.6(9)	103.0(5)	100.5(6)	102.9(5)	104.6(6)	104.1(5)
O3-Si2-O3'	108.1(9)	104.8(5)	104.3(7)	105.4(6)	110.9(7)	108.3(5)
O3-Si2-O8	112.4(6)	110.9(4)	111.8(5)	112.2(4)	111.2(5)	110.5(3)
O3-Si2-O9	103.3(6)	110.4(4)	111.5(5)	110.5(4)	108.9(5)	109.2(3)
O8-Si2-O9	116.5(9)	109.5(5)	106.1(8)	106.0(6)	105.6(7)	109.1(5)

O2-Si3-O2'	107.2(8)	105.9(5)	109.5(7)	107.1(6)	106.3(6)	107.1(5)
))))))
O2-Si3-O5	111.4(6)	111.8(4)	108.2(5)	109.5(4)	113.2(5)	110.8(3)
))))))
O2-Si3-O6	114.8(6)	115.5(4)	114.3(5)	114.8(4)	112.9(5)	114.1(3)
))))))
O5-Si3-O6	97.3(8)	96.4(5)	101.8(7)	100.9(5)	98.5(6)	99.9(5)
))))))
Si1-O9-Si2	165.5(11)	151.9(6)	148.5(8)	150.4(7)	151.4(7)	150.6(5)
))))))

* Abbreviations as in Table 1.